Journal of Solid State Chemistry 184 (2011) 109–114

Contents lists available at ScienceDirect

Journal of Solid State Chemistry

journal homepage: www.elsevier.com/locate/jssc

Enhanced thermoelectric performance and novel nanopores in $AgSbTe_2$ prepared by melt spinning

Baoli Du [a,b], Han Li [a], Jingjing Xu [a], Xinfeng Tang [a,*], Ctirad Uher [c]

[a] State Key Laboratory of Advanced Technology for Materials Synthesis and Processing, Wuhan University of Technology, Wuhan 430070, China
[b] School of Physics and Chemistry, Henan Polytechnic University, Jiaozuo 454000, China
[c] Department of Physics, University of Michigan, Ann Arbor, MI 48109, USA

ARTICLE INFO

Article history:
Received 23 July 2010
Received in revised form
18 October 2010
Accepted 31 October 2010
Available online 5 November 2010

Keywords:
$AgSbTe_2$
Rapid solidification
Nanopores
Thermoelectric property

ABSTRACT

We report a melt-spinning spark-plasma-sintering synthesis process of the polycrystalline *p*-type material composed of $AgSbTe_2$ coarse grains and evenly formed 5–10 nm pores that occur primarily on the surface of matrix grains. The formation mechanism of nanopores and their influences on the thermoelectric properties have been studied and correlated. Microstructure analysis shows that the as-prepared sample can be regarded as a nanocomposite of matrix and *in situ* generated nanopores evenly coated on matrix grains. For the single-phase component and the possible energy-filter effect caused by the nanopores, the electrical transport properties are improved. Moreover, the thermal conductivity is significantly reduced by strong phonon scattering effect resulted from the nanopores. The thermoelectric performance of the as prepared sample enhances greatly and a *ZT* of 1.65 at 570 K is achieved, increasing ~200% compared with the sample prepared by traditional melt and slow-cooling method.

1. Introduction

Thermoelectric energy conversion, by which heat is converted directly into electricity using a class of materials known as thermoelectric (TE) materials, is of great significance to alleviate the increasingly serious energy crisis and environmental problems [1–3]. High performance TE materials should possess the ideal TE properties of a phonon glass and an electron single crystal (PGEC) introduced by Slack [4] and Rowe [5]. That is high electrical conductivity σ, large Seebeck coefficient α and low thermal conductivity κ to retain the heat at the junction and to reduce the heat transfer losses.

In recent years, many experiments have confirmed that the PGEC transport property can be achieved in nanostructured bulk materials or materials with nano-scale inclusions [6–9]. Theory calculation indicates that the fine nanostructure would introduce quantum-confinement effects and carrier energy filtering effect to enhance the Seebeck coefficient and power factor $\alpha^2\sigma$ [10–12]. Moreover, the high-density nanograins boundary can lower the thermal conductivity by introducing extra strong phonon scattering effect without serious degradation of electrical conductivity [6,13], based on the mean free path differences of the phonons and carriers [14]. Hsu et al. [6] reported that $AgPb_{18}SbTe_{20}$ could achieve a record high *ZT* value of 1.7 at 700 K with nanocrystals of an Ag–Sb-rich phase embedded in a PbTe matrix. The nano-components can play an important role in scattering mid-to-long wavelength phonons, thus reducing the thermal conductivity.

$AgSbTe_2$ has been studied extensively as a *p*-type medium-temperature TE material [15–18] and as an end component of the two classes of high-performance TE material—$(AgSbTe_2)_{1-x}(GeTe)_x$ [5,19] and $(AgSbTe_2)_{1-x}(PbTe)_x$ [6,20]. The thermal conductivity of $AgSbTe_2$ compound is limited to a very low value (only 0.6–0.7 $W\,m^{-1}\,K^{-1}$) by its complex crystal structure, Ag/Sb disorder on cation sites and intrincally strong scattering of acoustic phonon modes by optic modes [21,22]. However, according to Ag_2Te–Sb_2Te_3 pseudo-binary phase diagram [23,24], $AgSbTe_2$ is a thermodynamic high temperature phase. So there are small amounts of unexpected impurities (such as Ag_2Te or Sb_2Te_3) in samples prepared by melt and slow-cooling method (MC) [17] and other synthesis methods [18,25–27]. In 2008, Wang et al. [25] prepared $AgSbTe_2$ compound with a *ZT* of 1.59 by mechanical alloying (MA). The high *ZT* value is attributed to the extremely low thermal conductivity resulting from the low relative density (approximately 80%) and the large pore percentage (approximately 13.9%).

In this paper, $AgSbTe_2$ compound was obtained by melt spinning (MS) of solidified ingots. For the ultrahigh cooling rate (about 10^4–10^6 $K\,s^{-1}$) [28], the high temperature phase is maintained to the maximum extent and the nanocrystalline would introduce in the resulted materials. In the last few years, it has been applied to several TE systems, such as filled skutterudites [8,29] and Bi–Te compounds [9,30], and a series of nanostructured materials are

* Corresponding author. Fax: +86 27 87860863.
E-mail address: tangxf@whut.edu.cn (X. Tang).

0022-4596/$ - see front matter © 2010 Elsevier Inc. All rights reserved.
doi:10.1016/j.jssc.2010.10.036

obtained. However, nanostructured $AgSbTe_2$ compound with novel nanopores prepared by MS were not reported yet. Song et al. [31] demonstrate that thermal conductivity of nanoporous bismuth thin films is much lower than solid nonporous samples due to the strong phonons scattering effect. Moreover, by coating a thin layer of nanopores on $AgSbTe_2$ matrix grains, an additional electron and phonon scattering mechanism may be introduced. In addition to helping reduce thermal conductivity by strong scattering the heat-carrying phonons, its selective scattering effect on charge carriers would introduce energy filtering effect and increase the Seebeck coefficient. Therefore, in this paper, polycrystalline bulk *p*-type $AgSbTe_2$ compound was prepared by MS combined with spark plasma sintering (SPS). The details of the technique and the results obtained are presented. The formation mechanism of nanopores and their influences on TE properties are studied.

2. Experimental

Starting materials were high purity Ag (99.995%, filament), Sb (99.9999%, shot) and Te (99.999%, shot) that were weighed and loaded into a carbon-coated silica tube. The tube was sealed under a pressure of 10^{-3} Pa, kept at 973 K for 10 h, and then quenched in a supersaturated brine. The obtained ingot was divided into two parts, one of which was grounded into powder, loaded into a graphite die and sintered by SPS for 5 min under vacuum to obtain bulk materials designated as SPS. The sintering temperature and pressure were 723 K and 35 MPa, respectively.

The other part of the ingot was melt spun to get the supercooled ribbon-shaped samples (designated as ribbons). The ingot was inserted into a quartz tube with a 0.35 mm diameter nozzle. In our MS apparatus, the ingot was inductively melted under the protection of the Ar atmosphere. The melt was ejected under a pressure of 0.02 MPa onto the outer surface of a chilled spinning copper roller (linear speed 10 m s^{-1}) where it was rapidly solidified in the form of thin ribbons. The ribbons were grounded into power and sintered by SPS to yield the bulk materials designated as MS-SPS. The sintering process parameters were the same as those mentioned above.

The samples were examined by powder X-ray diffraction (XRD, X'Pert PRO-PANalytical, Cu$K\alpha$) and the power compensation differential scanning calorimetry (DSC, TA, Q20). The fine microstructure of free fracture surfaces was observed by field emission scanning electron microscopy (FESEM, Hitachi, S-4800) with energy dispersive X-ray spectroscopy (EDX). The Hall coefficient R_H was measured by an Accent HL5500PC Hall measurement system using the van der Pauw method with a magnetic field of 5340 G. Adopting single-carrier model, the carrier concentration N and Hall mobility μ_H at room temperature were calculated from the formulas ($N=1/q\,R_H$, $\mu_H=R_H/\rho$, where e is the electron charge and ρ is the resistivity). Electrical conductivity σ and the Seebeck coefficient α were measured simultaneously by commercial equipment (ZEM-1, Ulvac, Inc.) in He atmosphere from 300 to 700 K. Thermal conductivities κ were calculated from the thermal diffusivity λ, specific heat C_p, and density d using the equation: $\kappa=\lambda C_p d$. The thermal diffusivity was measured by the laser flash method using the Netzsch LFA457 system. Specific heat was determined by differential scanning calorimetry using the TA Q20 system.

3. Results and discussion

3.1. Phase structure and microstructure

The actual compositions of sintered samples were examined using EDX on polished surfaces. The differences were within 2% compared to nominal formulas, fell within the expected range. Thus all samples are referred as their nominal compositions. Fig. 1 shows the XRD patterns of the SPS, ribbons and MS-SPS samples. The peaks are assigned to a cubic phase (*fcc* lattice, $Fm\bar{3}m$ group, formula $AgSbTe_2$) and no obvious peaks due to impurities that are often reported in the literature are detected [17,18,26]. Owing to the limited test accuracy, we cannot rule out the possibility of the presence of a very low density of impurities in those samples. In order to determine the phases of the obtained samples accurately, the DSC heat flow curves are shown in Fig. 2. For SPS sample, endothermic and exothermic peaks corresponding to the α–β phase transition of Ag_2Te are detected around 417 K [32,33] during the heating and cooling process, respectively. It means that there is a tiny amount of Ag_2Te impurity in SPS sample and the Ag_2Te impurity cannot disappear after the heating process. For the ribbons obtained after MS, the endothermic peak is observed in the heating process but there is no exothermic peak in the cooling process. The result indicates that the ribbons are multiphase materials, but the Ag_2Te impurity can dissolve into the matrix gradually in the heating process irreversibly. We speculate that it is related to the small grain size and the high reactivity of the grains in the ribbons. In addition, the DSC analysis implies that the MS-SPS sample is free of Ag_2Te impurity. Therefore, the MS process is of great importance to obtain single-phase polycrystalline $AgSbTe_2$ compound in the melt-quench-MS-SPS preparation route.

Fig. 3a–c shows FESEM photographs of the free side (a), wheel side (b), and cross-section (c) of the ribbons. 400–600 nm nanograins with fine surface texture (20–40 nm) are observed on the free side of the ribbons. On the wheel side, the size of nanograins spans from 20 to 100 nm. As shown in Fig. 3c, the grain size increase monotonously from wheel side to free side, due to the change of cooling rate. Owing to the ultrahigh nucleation rate without timely replenishment of melt during MS process, large amount of pores and gully-like structure are formed on both the free side and the wheel side of the ribbons. Fig. 3e, f shows FESEM photographs of the SPS (d) and MS-SPS (e, f) samples. respectively. For SPS sample, nanograins (20–50 nm) are evenly distributed at the grain boundaries. According to the DSC result and the pseudo-binary phase

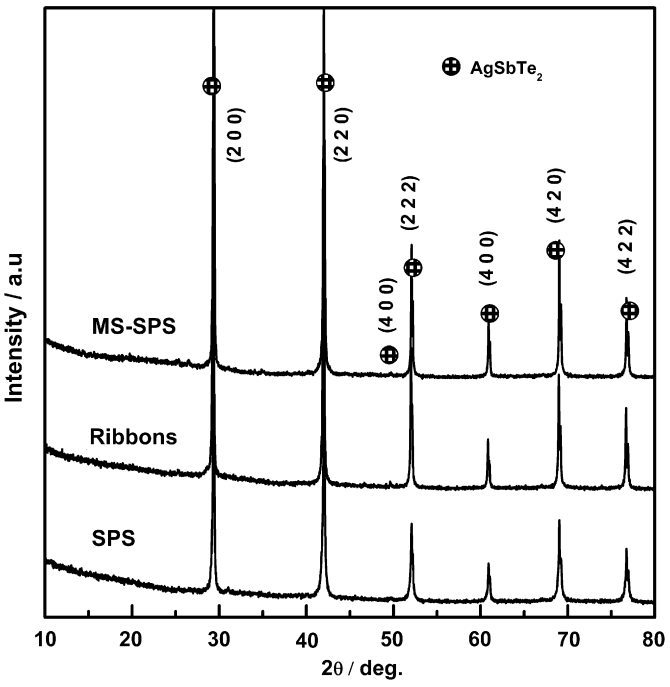

Fig. 1. XRD patterns of SPS, ribbons, and MS-SPS samples.

diagram [23], we deduce that the phase of the nanograins is Ag_2Te, in accord with the results reported in Refs. [17,18,25,27]. Unlike nanograins observed in SPS sample, uniformly distributed 5–10 nm pores were obtained on the surface of $AgSbTe_2$ matrix in MS-SPS sample, corresponding to the nanostructure characteristics of the ribbons.

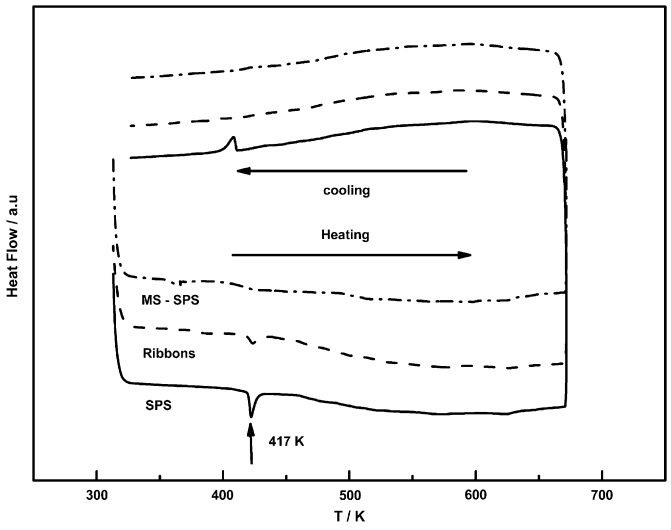

Fig. 2. DSC curves of SPS, Ribbons, MS-SPS samples (sample mass, 10 mg; heating/cooling rate, 20 K min^{-1}).

We attribute the different nanostructure of SPS and MS-SPS samples to the special MS process. For SPS sample, the Ag_2Te impurity in starting material (quenched ingots) diffuses from the inside of grains to the outside and reaches the grain boundaries during sintering process. Since the relatively low sintering temperature and short sintering time, the Ag_2Te has insufficient time to coarsen after nucleation and evolve into the evenly distributed 20–50 nm nanograins. However, the MS-SPS sample is obtained by sintering the ribbons achieved after MS. During sintering process, ribbon with a large effective surface area resulting from the surface texture lead to a enhanced reactivity towards secondary Ag_2Te phase. Therefore, the tiny amounts of Ag_2Te impurity dissolve into matrix quickly because of the high reactivity of the homogeneous nanocrystallines. Moreover, the surface texture of grains in ribbons have insufficient time to coarsen after evolving into dense bulk materials, so part of the pores and gully-like structure in ribbons are retained to the MS-SPS specimen and form a thin layer of 5–10 nm pores coated on the surface of $AgSbTe_2$ matrix. Compared with nanocomposites obtained by other method, the MS-SPS sample can be regarded as a nanocomposite composed of matrix grains and *in situ* generated nanopores. It is worth noting that the novel nanopores are achieved in a single phase material. Therefore,

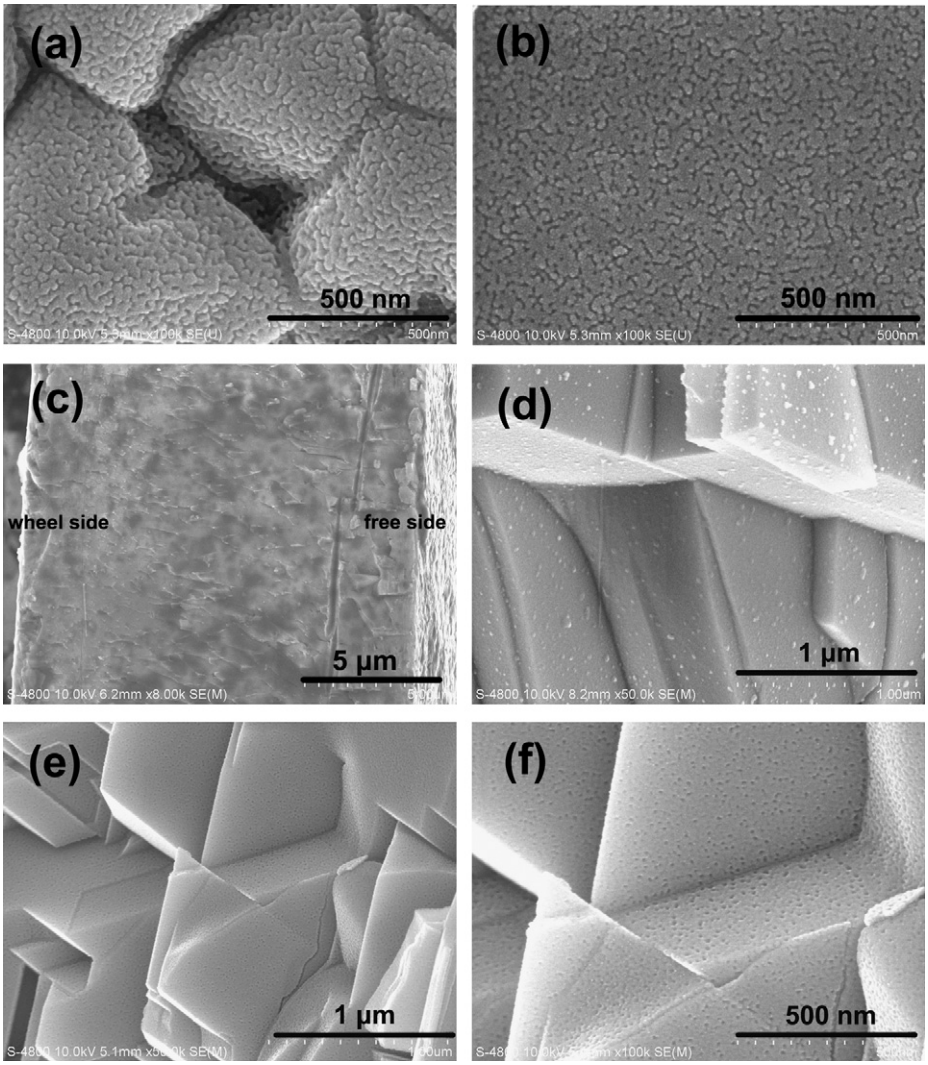

Fig. 3. FESEM photographs of Ribbon (a, free side; b, wheel side; c, cross-section), SPS (d), MS-SPS (e, low magnification; f, high magnification) samples.

the bad influences of the growth of nanograins in multiphase materials at relatively high temperature may be prevented.

3.2. Electrical transport properties

The temperature dependence of the electrical conductivity σ and the Seebeck coefficient α for MS-SPS sample and reference samples are shown in Fig. 4. The electrical conductivity of MS-SPS sample increases with the increasing temperature and reaches a maximum of 2.0×10^4 S m^{-1} at$\sim$665 K, much higher than that of the MA sample [25] with low relative density and higher than that of the SPS sample above 380 K. However, it is lower than that of the samples prepared by the traditional MC method, which may be ascribed to the impurities with high electrical conductivity (such as Ag_2Te and Sb_2Te_3) in the MC sample [17]. The MS-SPS sample exhibits positive Seebeck coefficient (shown in Fig. 4b) as SPS sample with nano-Ag_2Te evenly distributed on the matrix grain surface [18]. The value of α is above 255 μV K^{-1} in the whole measured temperature range and reaches its maximum of 285 μV K^{-1} at$\sim$390 K. At room temperature, the Seebeck coefficient of MS-SPS sample is 2.5 times higher than that of the MC (75 μV K^{-1}) sample [17], and is similar to that of MA sample (260 μV K^{-1}) [25]. However, the Seebeck coefficient of MS-SPS sample is similar to the high quality single-phase samples prepared by conventional solid state chemistry without invoking more exotic manufacturing methods [16]. In this Ref. [16], only XRD pattern is shown to certify the single-phase of the as prepared sample. Take the limited accuracy of the XRD into account, we cannot rule out the possibility of the presence of a very low density of impurities in those samples. Furthermore, According to the numerous papers about $AgSbPb_mTe_{2+m}$ (LAST) [6] and PbTe compounds [34] reported by Kanatzidis group, we think that the sample reported by Jojovic et al. should have nanostructure in bulk $AgSbTe_2$ material, and the large Seebeck coefficient may relate to the carrier energy filtering effect aroused by the fine nanostructure.

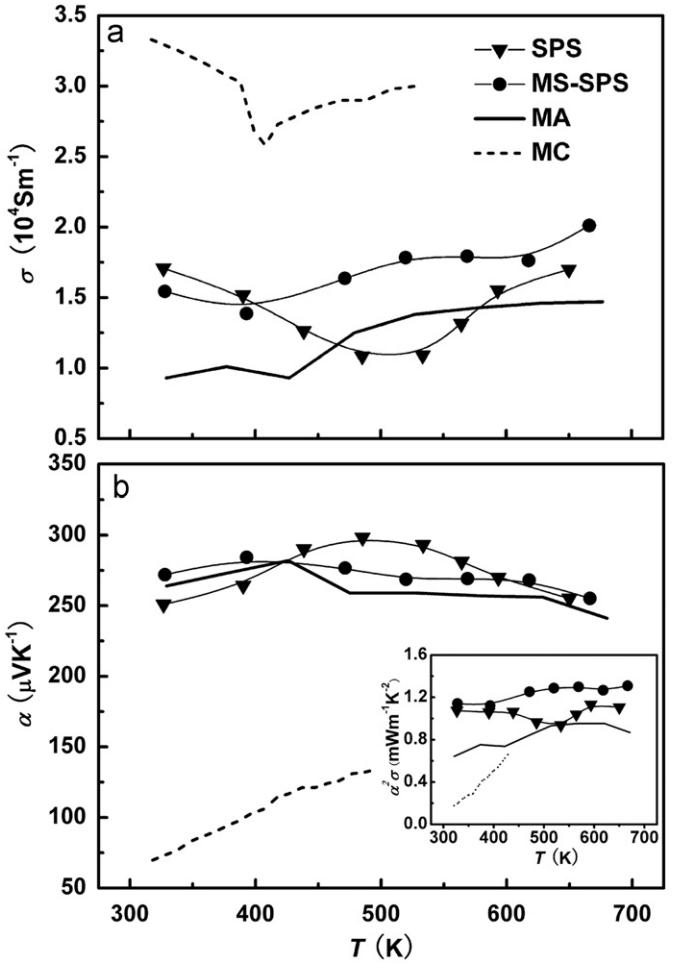

Fig. 4. Temperature dependence of electrical conductivity (a), Seebeck coefficient (b) and power factor (inset of Fig. 4b) for MS-SPS and reference samples. Lines are plotted as a guide to the eye.

In general, the Seebeck coefficient α of degenerate semiconductors as a function of the energy dependence of the electrical conductivity $\sigma(E)$ can be given by Mott relation [35]:

$$\alpha=\frac{\pi^2}{3}\frac{k_B^2}{e}\left\{\frac{d[\ln(\sigma(E))]}{dE}\right\}_{E=E_F} \quad (1)$$

where the electrical conductivity is $\sigma=\sigma(E_F)$. E, e, and k_B are carrier energy, electron charge, and Boltzmann constant, respectively. In addition, for solids with parabolic bands, an energy dependence on relaxation time τ is customarily introduced: $\tau=\tau_0E^{\lambda-1/2}$, where λ is scattering factor [36]. Combining with the equations $\sigma=ne\mu=ne^2\tau/m^*$ (n, μ, and m^*, are carrier density, Hall mobility, and the density-of-states effective mass, respectively), Seebeck coefficient for a given carrier density increases as the scattering factor increases. According to the Hall measurement, MS-SPS sample has the similar carrier density (6×10^{19} cm^{-3}) as MC sample (5×10^{19} cm^{-3}). Therefore, the increased Seebeck coefficient should be attributed to an increased scattering factor, presumably from the potential barrier scattering effect [37] aroused by the 5–10 nm pores, similar to the increase of Seebeck coefficient in SPS sample by evenly distributed 20–50 nm Ag_2Te nanograins [18,38]. Similar results have been reported in PbTe-based [34,39], ZrNiSn-based [40] and filled skutterudite-based nanocomposite materials [41]. Therefore, a conclusion can be drawn: the nanopores can introduce an additional scattering mechanism which preferentially scatters low energy electrons as nanograins embedded in the matrix, minimizing their contribution to transport properties and thus increasing the Seebeck coefficient [14]. The inset of Fig. 4b presents the temperature dependence of power factor $\alpha^2\sigma$ for MS-SPS sample and reference samples. The value of $\alpha^2\sigma$ for MS-SPS sample reaches 1.3 mW K^{-2} m^{-1} at$\sim$665 K, which is much higher than those of SPS, MA, and MC samples. The above results indicate that MS-SPS sample can exhibit high electrical conductivity without sacrifice of the Seebeck coefficient.

3.3. Thermal transport properties

The temperature dependence of thermal conductivities κ and the lattice thermal conductivities κ_L for MS-SPS sample and reference samples are shown in Fig. 5. The thermal conductivity of MS-SPS sample is 20–60% lower than those of SPS and MC samples, respectively. Moreover, though MS-SPS sample processes nearly theoretical density, the value of κ does not increase too much compared with that of MA sample with low relative density.

To further investigate the influence of the nanopores on thermal transport properties, lattice thermal conductivity κ_L is calculated using the Wiedemann–Franz law:

$$\kappa_L=\kappa-L\sigma T \quad (2)$$

where $L=0.7L_0$ [16,42], $L_0=\pi^2/3(k_B/e)^2=2.45\times10^{-8}V^2/K^2$ (shown in the inset of Fig. 5a). At room temperature, the lattice thermal conductivity of MS-SPS sample (0.42 W m^{-1} K^{-1}) is 35% lower than that of MC sample (0.65 W m^{-1} K^{-1}), and a minimum of 0.30 W m^{-1} K^{-1} is reached at $\sim$570 K, closing to the minimum theoretical thermal conductivity ($\sim$0.3 W m^{-1} K^{-1}) calculated from formulas reported by Cahill et al. [43].

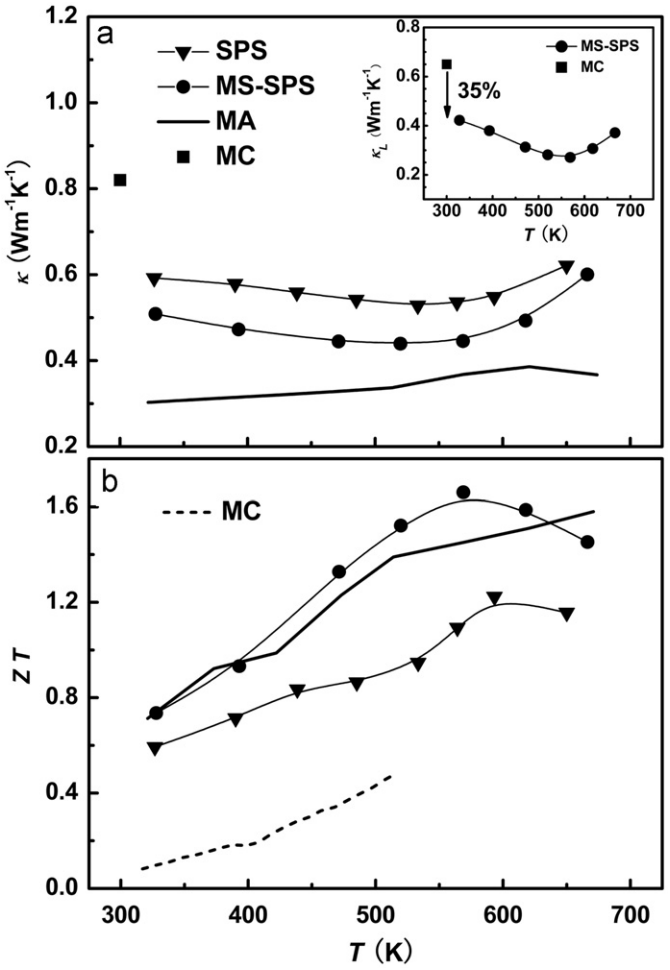

Fig. 5. Temperature dependence of thermal conductivity (a), lattice thermal conductivity (inset of Fig. 5a) and figure of merit *ZT* (b) for MS-SPS and reference samples. Lines are plotted as a guide to the eye.

In the traditional diffusion–approximation based Maxwell-Garnett's model [44,45], the bulk thermal conductivity of a porous materials is only a function of the pore volume fraction ϕ:

$$\kappa_{eff} \approx \kappa_m[2(1-\phi)/(2+\phi)] \quad (3)$$

where κ_m is the bulk thermal conductivity of the host medium. Assuming $\phi=0$ for MC sample [17], the lattice thermal conductivity of MS-SPS sample is as low as that of sample with porosity $\phi=27\%$ prepared by traditional MC method. Therefore, the diffusion–approximation based effective medium models cannot be used to predict the thermal conductivity of MS-SPS sample, since the pore size can be comparable to the mean free path of phonons [46]. Strictly speaking, the Boltzmann transport equation must be solved to capture the ballistic nature of thermal transport and phonon size effects due to the small pore diameter. Therefore, the 5–10 nm pores can act as scattering center of heat-carrying phonons and notably enhance grain boundaries scattering effects on phonon behavior, and resulting in the reduction of the thermal conductivity.

3.4. Figure of merit ZT

The temperature-dependent figures of merit for MS-SPS sample calculated from the above data are compared in Fig. 5b with the values reported for samples prepared by other methods. As the temperature increases, the figure of merit of MS-SPS sample initially rapidly increases and reaches a maximum of 1.65 at temperatures ~570 K, increased by ~35%, ~200% compared with the SPS and the MC samples, respectively. It is worth noting that the *ZT* of $AgSbTe_2$ already has exceeds 1.0 at 400 K. Therefore, due to the high power factor and low thermal conductivity, the bulk $AgSbTe_2$ material evenly coated with nanopores seems to exhibit high TE performance over a wide temperature range.

4. Conclusion

In conclusion, the highly pure $AgSbTe_2$ compound with 5–10 nm nanopores evenly coated on the surface of the matrix gains is obtained benefiting from the ultrahigh cooling rate of melt-spinning process and spark plasma sintering rapid densification. MS-SPS sample exhibits similar Seebeck coefficient and higher electrical conductivity compared with samples prepared by melt-quench-SPS and MA method. The thermal conductivity is greatly reduced due to the strong phonon scattering effects resulted from 5 to 10 nm pores. As a result, the TE performance of MS-SPS sample improves remarkably and a *ZT* of 1.65 is achieved at ~570 K, which increases ~35% and ~200% compared with sample prepared by melt-quench-SPS and traditional melting and slow-cooling method. Our study suggests that nanopores introduce a new scattering mechanism and have great impact on electron and phonon transport properties, and it is fair to consider it as a new paradigm for designing and optimizing thermoelectric materials.

Acknowledgments

Baoli Du thanks Wenjie Xie for his constructive discussions. This work is sponsored by the National Basic Research Program of China (Grant No. 2007CB607501), the National Science Foundation of China (Grant Nos. 50820145203 and 50731006) and 111 Project (Grant No. B07040). Work of CU is supported by a grant from the University Research Corridor.

References

[1] T.M. Tritt, M.A. Subramanian, MRS Bull. 31 (2006) 188–194.
[2] L.E. Bell, Science 321 (2008) 1457–1461.
[3] J. Yang, F. Stabler, J. Electron. Mater. 38 (2009) 1245–1251.
[4] G.A. Slack, MRS Bull. 23 (1998) 15–21.
[5] D.M. Rowe, Handbook of Thermoelectrics Macro to Nano, CRC, Boca Raton, FL, 2006.
[6] K.F. Hsu, S. Loo, F. Guo, W. Chen, J.S. Dyck, C. Uher, T. Hogan, E.K. Polychroniadis, M.G. Kanatzidis, Science 303 (2004) 818–821.
[7] D.J. Singh, I. Terasaki, Nat. Mater. 7 (2008) 616–617.
[8] H. Li, X. Tang, Q. Zhang, C. Uher, Appl. Phys. Lett. 93 (2008) 252109.
[9] W.J. Xie, X.F. Tang, Y.G. Yan, Q.J. Zhang, T.M. Tritt, Appl. Phys. Lett. 94 (2009) 102111.
[10] L.D. Hicks, M.S. Dresselhaus, Phys. Rev. B 47 (1993) 12727–12731.
[11] W. Kim, J. Zide, A. Gossard, D. Klenov, S. Stemmer, A. Shakouri, A. Majumdar, Phys. Rev. Lett. 96 (2006) 045901.
[12] D. Vashaee, A. Shakouri, Phys. Rev. Lett. 92 (2004) 106103.
[13] G.H. Zhu, H. Lee, Y.C. Lan, X.W. Wang, G. Joshi, D.Z. Wang, J. Yang, D. Vashaee, H. Guilbert, A. Pillitteri, M.S. Dresselhaus, G. Chen, Z.F. Ren, Phys. Rev. Lett. 102 (2009) 196803.
[14] A.J. Minnich, M.S. Dresselhaus, Z.F. Ren, G. Chen, Energy Environ. Sci. 2 (2009) 466–479.
[15] L.H. Ye, K. Hoang, A.J. Freeman, S.D. Mahanti, J. He, T.M. Tritt, M.G. Kanatzidis, Phys. Rev. B 77 (2008) 245203.
[16] V. Jovovic, J.P. Heremans, Phys. Rev. B 77 (2008) 245204.
[17] K.T. Wojciechowski, M. Schmidt, Phys. Rev. B 79 (2009) 184202.
[18] J. Xu, H. Li, B. Du, X. Tang, Q. Zhang, C. Uher, J. Mater. Chem. 20 (2010) 6138–6143.
[19] S.H. Yang, T.J. Zhu, T. Sun, J. He, S.N. Zhang, X.B. Zhao, Nanotechnology 19 (2008) 245707–245711.
[20] X.Z. Ke, C.F. Chen, J.H. Yang, L.J. Wu, J. Zhou, Q. Li, Y.M. Zhu, P.R.C. Kent, Phys. Rev. Lett. 103 (2009) 145502.
[21] S.V. Barabash, V. Ozolins, C. Wolverton, Phys. Rev. Lett. 101 (2008) 155704.
[22] D.T. Morelli, V. Jovovic, J.P. Heremans, Phys. Rev. Lett. 101 (2008) 035901.
[23] G. Petzow, G. Effenberg, Ternary Alloys 2 (1988) 554–556.

[24] R.-M. Marin, G. Brun, J.-C. Tedenac, J. Mater. Sci. 20 (1985) 730–735.
[25] H. Wang, J.F. Li, M.M. Zou, T. Sui, Appl. Phys. Lett. 93 (2008) 202106.
[26] R. Wolfe, J. Wernick, S. Haszko, J. Appl. Phys. 31 (1960) 1959–1964.
[27] T.C. Su, X.P. Jia, H.A. Ma, F.R. Yu, Y.J. Tian, G.H. Zuo, Y.J. Zheng, Y.P. Jiang, D. Dong, L. Deng, B. Qin, S.Z. Zheng, J. Appl. Phys. 105 (2009) 073713.
[28] A.G. Gillen, B. Cantor, Acta Metall. 33 (1985) 1813–1815.
[29] H. Li, X. Tang, X. Su, Q. Zhang, C. Uher, J. Phys. D: Appl. Phys. 42 (2009) 145409.
[30] W. Xie, X. Tang, Y. Yan, Q. Zhang, T. Tritt, J. Appl. Phys. 105 (2009) 113713.
[31] D.W. Song, W.N. Shen, B. Dunn, C.D. Moore, M.S. Goorsky, T. Radetic, R. Gronsky, G. Chen, Appl. Phys. Lett. 84 (2004) 1883–1885.
[32] S.S. Ragimov, S.A. Aliev, Inorg. Mater. 43 (2007) 1184–1186.
[33] F. Kracek, C. Ksanda, L. Cabri, Am. Mineral. 51 (1966) 14–28.
[34] J.R. Sootsman, H. Kong, C. Uher, J.J. D'Angelo, C.I. Wu, T.P. Hogan, T. Caillat, M.G. Kanatzidis, Angew. Chem. Int. Ed. 47 (2008) 8618–8622.
[35] N.F. Mott, E.A. Davis, Electronic Processes in Non-crystalline Materials, Clarendon, Oxford, 1979.
[36] J.P. Heremans, C.M. Thrush, D.T. Morelli, J. Appl. Phys. 98 (2005) 063703.
[37] L.I. Bytenskii, T.S. Gudkin, E.K. Iordanishvili, S.A. Kaz'min, V.I. Kaidanov, S.A. Nemov, Y.I. Ravich, Semiconductors 11 (1977) 894–896.
[38] B. Du, J. Xu, W. Zhang, X. Tang, J. Electron. Mater. (2010), under review.
[39] K. Kishimoto, M. Tsukamoto, T. Koyanagi, J. Appl. Phys. 92 (2002) 5331–5339.
[40] L.D. Chen, X.Y. Huang, M. Zhou, X. Shi, W.B. Zhang, J. Appl. Phys. 99 (2006) 064305.
[41] Z. Xiong, X.H. Chen, X.Y. Huang, S.Q. Bai, L.D. Chen, Acta Mater. 58 (2010) 3995–4002.
[42] S.N. Zhang, T.J. Zhu, S.H. Yang, C. Yu, X.B. Zhao, Acta Mater. 58 (2010) 4160–4169.
[43] D.G. Cahill, S.K. Watson, R.O. Pohl, Phys. Rev. B 46 (1992) 6131–6140.
[44] H. Szelagowski, I. Arvanitidis, S. Seetharaman, J. Appl. Phys. 85 (1999) 193–198.
[45] J.C. Maxwell-Garnett, Philos. Trans. R. Soc. 203 (1904) 385–420.
[46] R. Prasher, J. Appl. Phys. 100 (2006) 064302.